J Mater Sci (2008) 43:671–679
DOI 10.1007/s10853-007-2160-2

Microstructure and properties of ultrafine-grained and dispersion-strengthened titanium materials for implants

D. Handtrack · C. Sauer · B. Kieback

Received: 10 March 2007 / Accepted: 10 September 2007 / Published online: 17 October 2007

Abstract Wear-resistant titanium materials with high hardness and strength can be manufactured by introducing very fine titanium silicides and carbides into an ultrafine-grained titanium matrix. Nanocrystalline titanium particles with fine and homogeneous distributed carbon and silicon were generated by high energy ball milling of titanium with silicon powder or additions of the organic fluid hexamethyldisilane (HMDS). Spark Plasma Sintering (SPS) was chosen to compact the granules to prevent grain coarsening during sintering. Additionally, the Ti_5Si_3 and TiC_x dispersoids limited grain coarsening. After sintering, the novel materials exhibited high hardness and strength, and excellent wear resistance. The electrochemical behaviour (comparable to that of commercially pure titanium) was also tested and showed the excellent suitability as an implant material.

Introduction

Titanium is well-suited as a metallic implant material due to its superior biocompatibility in comparison to other metals [1, 2]. However, disadvantages for the use of commercially pure (c.p.) Ti as an implant material are its low strength, insufficient hardness and low wear resistance. Until now, improvement of these mechanical and tribological properties of titanium materials has been obtained by alloying and, in particular, by coatings. Both methods have certain disadvantages. In the case of alloying the presence of some alloying, elements can cause cell toxic or allergic effects. On the other hand, wear-reducing coatings on titanium implants tent to flake off.

A new approach for a significant improvement in the strength and hardness of titanium implants is to develop ultrafine-grained and dispersion-strengthened titanium materials. The dispersoids are used to reduce the grain growth during the technologically necessary heat treatment and to increase the strength and hardness via interaction with dislocations. Titanium silicides and titanium carbides are well-suited as dispersoids because they do not appear to affecting the favourable TiO_2 passive layer, and no harmful effects of Si and C on the human body tissue are known.

A suitable method to achieve the desired ultrafine-grained and dispersion strengthened microstructure is the high energy ball milling process of powder mixtures [3]. Nanocrystalline powder granules can be produced. To maintain the nanocrystalline microstructure during the subsequent densification, a sintering technique must be used, which allows the manufacture of almost dense materials at low sintering temperatures and short sintering times. A technique that meets these requirements is Spark Plasma Sintering (SPS). In this method, the powder compacts are heated to sintering temperature by a pulsed electric current under vacuum conditions. Surface activation of the powder granules occurs, and subsequent plastic flow at the particle contacts is caused by the simultaneous pressure impact [4]. By this means, almost dense titanium materials with an ultrafine-grained microstructure can be manufactured by using high heating rates, low sintering

D. Handtrack (✉) · C. Sauer · B. Kieback
Technische Universitaet Dresden, Institute of Materials Science, Dresden, Germany
e-mail: dirk_handtrack@web.de

Present Address:
D. Handtrack
PLANSEE SE, Innovation Services, Reutte, Austria

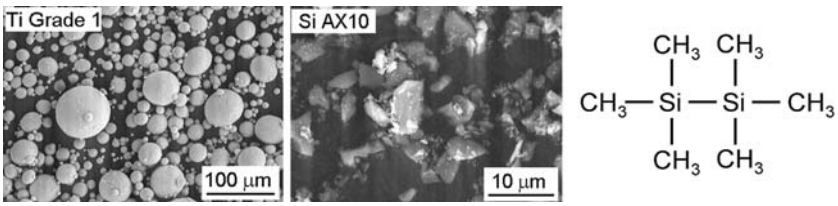

Fig. 1 SEM micrographs of the starting powders Ti and Si, and structural formula of HMDS

temperatures and short sintering times in comparison to conventional sintering methods.

Experimental

Materials processing

The appropriate microstructure consisting of an ultrafine-grained titanium matrix with very fine dispersoids is obtained by high energy ball milling of powder mixtures in a RETSCH planetary ball mill PM400 [5]. A 45 g mixture of gas atomized titanium powder, d_{50}=45 µm, with 1 wt.% of silicon powder, d_{50}=4.4 µm, (Ti/1Si) was used as starting material in the first experiments (Fig. 1). Mixtures of titanium powder and an organic fluid as carrier for the dispersoid forming elements Si and C were used. Hexamethyldisilane (HMDS) was well suited for this application (Fig. 1). The compositions Ti with 1.3 wt.% of HMDS (Ti/1.3HMDS), corresponding to 0.5 wt.% Si, 0.65 wt.%C and 2.6 wt.% of HMDS (Ti/2.6HMDS), corresponding to 1 wt.% Si, 1.3 wt.% C (Ti/1.6HMDS) were used as starting materials for the milling process.

The blends were milled for 64 h with 150 rpm under argon atmosphere. Milling vial and 10 mm-balls were made of stainless steal, the powder-to-ball-mass ratio was 1:10. At these conditions, nanocrystalline powder granules have been obtained. For Ti/1.3HMDS and Ti/2.6HMDS, a heat treatment at 400 °C under high vacuum conditions was necessary to remove the hydrogen introduced by HMDS from the titanium material. The holding periods of degassing were determined at 30 min for Ti/1.3HMDS and 60 min for Ti/2.6HMDS respectively. The compaction of the powder granules was performed using laboratory SPS equipment Dr. Sinter SPS5155 (Sumitomo Coal Mining Company). The pressure was 80 MPa. A heating rate of 100 K min^{-1}, a sintering temperature of 700 °C and a sintering time of 6 min were necessary to obtain titanium materials with a relative density of 99.6 % [6]. The average titanium matrix grain size d_{50} after compaction was in a range of 300–500 nm. XRD investigations show that the dispersoid formation of Ti_5Si_3 and TiC_x occurs by diffusion of the elements Si and C introduced by the HMDS into the titanium matrix [7]. The calculated volume fractions of dispersoids of the novel titanium materials after sintering are shown in Table 1.

Table 1 Dispersoid volume fractions for the new titanium materials; calculated from the starting composition

	Ti/1Si	Ti/1.3HMDS	Ti/2.6HMDS
Ti_5Si_3	4 vol.%	2 vol.%	4 vol.%
TiC_x	–	4 vol.%	8 vol.%

Characterization

A hardness tester HMV2000 and an universal testing machine Zwicki 005 were used to determine the Vickers hardness HV0.5 and the mechanical properties via three-point bending tests, respectively.

To investigate the influence of the increased hardness and strength on the wear resistance of the new materials, wear tests were performed by using the pin-on-disc model. Due to the limitations for the sample geometry in the SPS process, only pins of the new materials could be manufactured. Primary c.p. Ti was used as disc material with respect to investigating the biocompatibility of the wear particles. In addition, the harder and technically more relevant implant alloy TiAl6V4 was applied as the disc material. The investigations were performed on a tribometre TRM 1000. The tests ran for max. 20 h at 37 °C in Ringer's solution (0.147 mol/l NaCl, 0.004 mol/l KCl, 0.0022 $CaCl_2 \cdot H_2O$) to simulate the conditions of an implant environment, the speed was 0.1 m/s, the surface pressure was 2 MPa. Termination condition was chosen by a wear limit of 0.7 mm. To evaluate the wear behaviour of the new materials Ti/1Si, Ti/1.3HMDS and Ti/2.6HMDS, samples of SPD-c.p. Ti (grade 4; manufactured by severe plastic deformation; ECAP—equi channel angular pressing, n = 8), c.p. Ti and TiAl6V4 were also tested.

To characterize the biocompatibility of the wear particles generated by the tribological tests, the interaction of the material with humane endothelial cells was investigated with regard to pro-inflammatory reactions (ICAM-1, IL-8) and cell vitality (MTS conversion, cell number). To prevent the influence of alloying elements from the disc material (e.g., vanadium from TiAl6V4 discs), only wear particles produced vs. c.p. Ti discs were used.

Potentio-dynamic measurements up to 10 V_{SCE} and serial electrochemical impedance spectroscopy (EIS) in phosphate buffered saline (PBS, pH = 7.4) at 37 °C were

performed to characterize the corrosion behaviour and the conductivity of the passive layers of the new titanium materials in comparison to c.p. Ti. EIS was carried out at potentials between –300 mV_{SCE} and 1,000 mV_{SCE} in 50 mV-steps and frequency ranges of 10 mHz–10 kHz, the oscillation amplitude was 10 mV. According to literature, the software EQUIVCRT [8] and an equivalent circuit diagram [9] were used to evaluate these measurements.

The cross sections for microstructural analysis with a TEM EM 912 Omega have been prepared by T-tool® technique [10] and a following ion milling in a Gatan Duo Mill 600. A TEM Tecnai F30 with a HDAAF combined with EDX and EELS was used for analytical investigations of specimens prepared by FIB technique.

Results

Mechanical performance and microstructure

The yield curves generated in three-point bending tests show the superior strength of the novel materials in comparison to that of c.p. Ti manufactured by SPS of the unmilled titanium starting powder (Fig. 2). Yield strength, bending strength and hardness have clearly been improved by the mechanisms of grain size refinement and dispersion-strengthening (Table 2). Furthermore, it can be seen that the new material Ti/1.3HMDS is characterized by an acceptable plastic elongation.

We assume that the reason for the good ductility of Ti/1.3HMDS is due to the grain size and grain size distribution as shown in Fig. 3. Its microstructure is characterized by a wide grain size distribution with areas of very fine grains (40 nm) next to areas with coarser grains (≈1,000 nm).

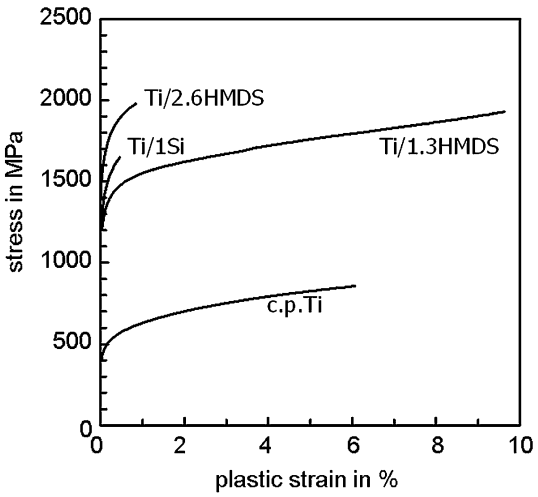

Fig. 2 Yield curves of the novel titanium materials and c.p. Ti generated in three-point bending tests

The statistic evaluation by linear analysis gives the grain size distribution for Ti/1.3HMDS shown in Fig. 4. A 25% volume fraction of grains is in the range between 500 nm and 1,000 nm embedded in a matrix of smaller grains with a large spread of 40–500 nm in size.

It is assumed that the deformation behaviour can be explained by the mechanisms acting for metallic ultrafine-grained materials with a bimodal grain size distribution. Thus, larger grains deform by the common mechanisms of dislocation movement and strain hardening, while fine grains lead to a significant increase in the material hardness and strength, as expected from an extrapolation of the Hall–Petch relationship [11]. The combination of good ductility and high strength based on a bimodal grain size distribution is already reported and discussed for aluminium and copper alloys manufactured by powder metallurgical processes [12, 13].

In the present work, it is assumed that the volume fraction of coarser grains (>500 nm) causes the ductility increase, while the finer grains (<500 nm) contribute to the increase in strength. The material Ti/2.6HMDS contains a higher amount of dispersoids (ref. Table 1), which are predominantly located at grain boundaries. Although Ti/1.3HMDS exhibits relatively poor homogeneity of the dispersoids, the distribution of the dispersoids in Ti/2.6HMDS is more homogeneous, and thus prevents grain coarsening during sintering (Fig. 3). The finer Ti matrix grain size (maximum value 673 nm) and the presence of only few coarser grains are the reasons for the limited plastic deformation behaviour of Ti/2.6HMDS.

The reasons of the lower ductility of Ti/1Si in comparison to the other materials tested are the significantly coarser dispersoids and their morphologies (cp. Figs. 3, 5, 6). The angular Ti_5Si_3 dispersoids are in a size range of 200–300 nm and can lead to crack-initiating stress concentrations during deformation. As mentioned above, these specimens were produced by milling and SPS of a Ti–Si powder mixture.

The contiguous Ti_5Si_3 and TiC_x dispersoids in Ti/1.3HMDS and Ti/2.6HMDS are spherical in shape and significantly smaller, averaging about 150 nm (Figs. 3, 6). In contrast to Ti/1Si, these specimens were produced by milling and SPS of Ti powder with the organic Si-precursor.

We assume that a fine and homogeneous distribution of Si- and C-containing molecules by a mechano-chemical decomposition of HMDS influences the dispersoid formation in the subsequent sintering process in contrast to the larger Si particles in the milled Ti–Si powder mixture. It is assumed that during deformation, there is a much lower local stress around the particles in Ti/HDMS due to their smaller size and spherical shape. This may explain the increased plastic elongation.

Table 2 Mechanical properties of the new titanium materials and c.p. Ti

	c.p.Ti	Ti/1Si	Ti/1.3HMDS	Ti/2.6HMDS
Hardness [HV 0.5]	160 ± 11	359 ± 32	319 ± 25	350 ± 21
Yield strength* [MPa]	477 ± 15	1,305 ± 169	1,439 ± 111	1,541 ± 80
Bending strength [MPa]	829 ± 30	1,548 ± 144	2,018 ± 105	1,830 ± 104
Plast. elong. at break [%]	6.1 ± 0.4	0.6 ± 0.2	7.1 ± 2.3	1.0 ± 0.4

* defined for 0.1 % plastic elongation

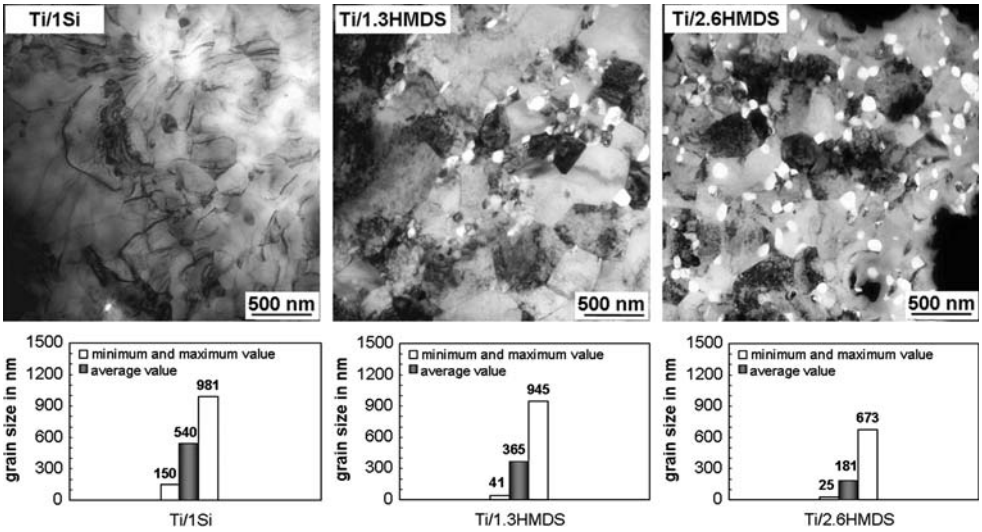

Fig. 3 TEM micrographs and titanium matrix grain sizes of the new titanium materials

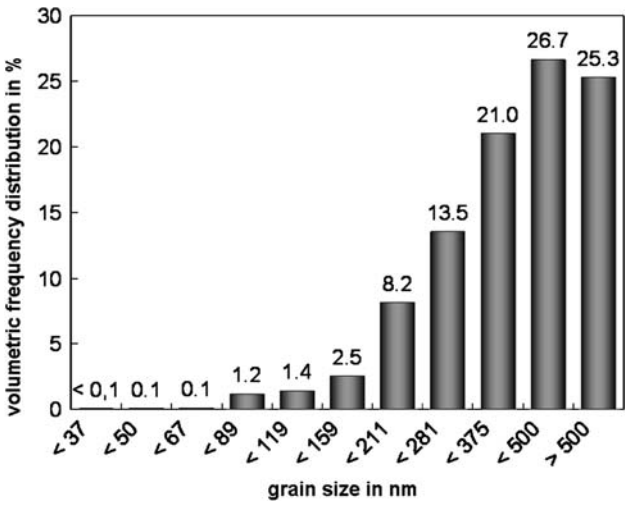

Fig. 4 Volumetric grain size distribution of the titanium matrix in Ti/1.3HMDS

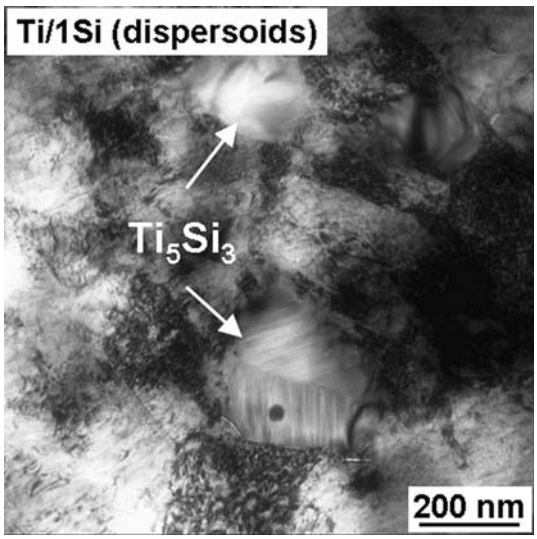

Fig. 5 TEM micrographs for Ti/1Si showing Ti_5Si_3 dispersoids

Wear behaviour

In Fig. 7, it can be seen that the embedded dispersoids reduce wear depending on amount and size. Additionally, the different wear behaviour depending on the disc materials can clearly be observed. The wear rates vs. the c.p. Ti-disc are significantly higher than those versus the TiAl6V4-disc. The distinct cold welding behaviour between c.p. Ti and the tested pin materials promotes the adhesive wear and leads to an obvious material transfer from the disc to the pin (Fig. 8). After the tests, a periodic sequence of dispersoid-free and dispersoid-containing areas were observed (Fig. 9). We assume that during the wear test, there is an alternating material transfer onto the

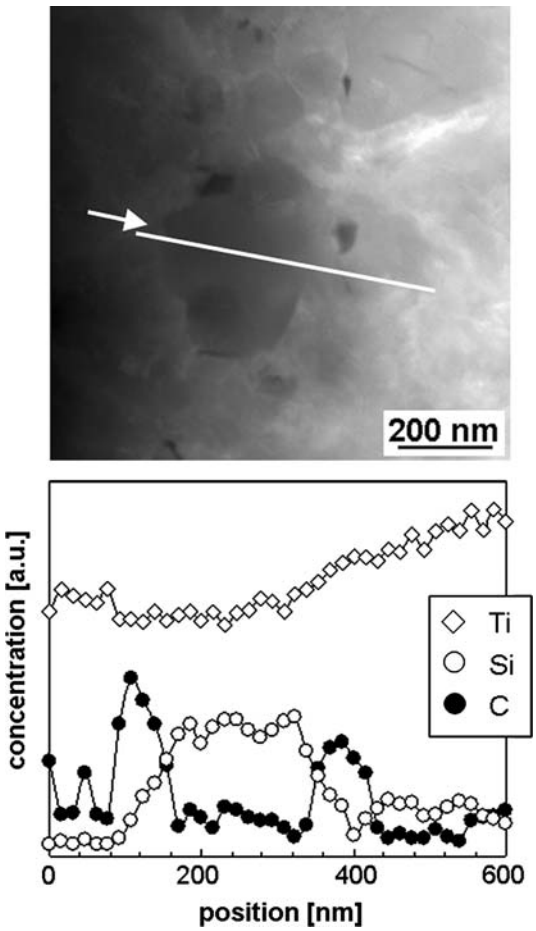

Fig. 6 Ti-, Si- and C-concentration profiles in Ti/2.6HMDS

stressed pin surface from worn c.p. Ti particles on one hand and from dispersoid containing pin particles on the other hand.

Furthermore, a grain size refinement close to amorphization was verified by TEM electron diffraction investigations made before and after the wear tests (Fig. 10). Both grain size refinement and the welding of the hard, dispersoids-containing wear particles cause a significant hardness increase in the tribological tests, reflected in the change of the wear rates during the tests vs. the c.p. Ti disc. The observed wear layer grows during the run-in period (high wear rate). After the hardening of the surface, the wear rate decreases clearly. The run-in period of the tested materials depends significantly on the composition and the microstructure, respectively (volume content and size of the dispersoids).

Despite the higher hardness with the TiAl6V4 disc material, lower wear rates were obtained due to the less pronounced adhesion behaviour of the α-β-alloy in comparison to c.p. Ti (Fig. 8). All the newly developed materials exhibited similar wear behaviour independent of the composition, and with no influence of the volume fraction or size of the dispersoids.

In contrast to the cumulative wear of the pin and disc displayed in Fig. 7, the pin length decrease was determined for the calculation of the wear coefficients k_w for the stable wear by Eq. 1, where A is the cross section of the pin, Δl is the decrease in the pin length, F is the contact force between the pin and the disc, and s is the total sliding distance, to characterize the wear behaviour of the new titanium materials.

$$k_w = \frac{A \cdot \Delta l}{F \cdot s} \tag{1}$$

Figure 11 shows results from wear tests confirmed by a second sample of the same material. Since each pair of specimens performed in a similar manner, the result of only one specimen is presented. The novel ultrafine-grained and dispersion strengthened titanium materials show a superior wear resistance compared to c.p. Ti and TiAl6V4. The impact of grain size refinement on the wear behaviour can be described by comparing c.p. Ti with SPD-c.p. Ti; the influence of the dispersoids can be seen by comparing

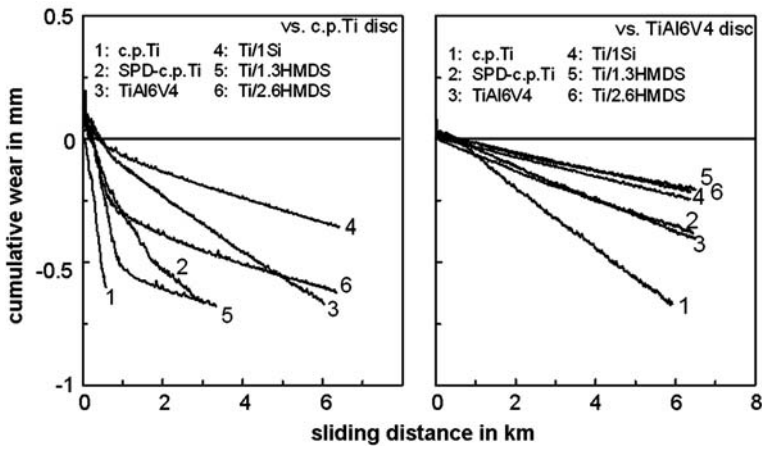

Fig. 7 Wear curves of titanium materials tested versus c.p. Ti and TiAl6V4 discs

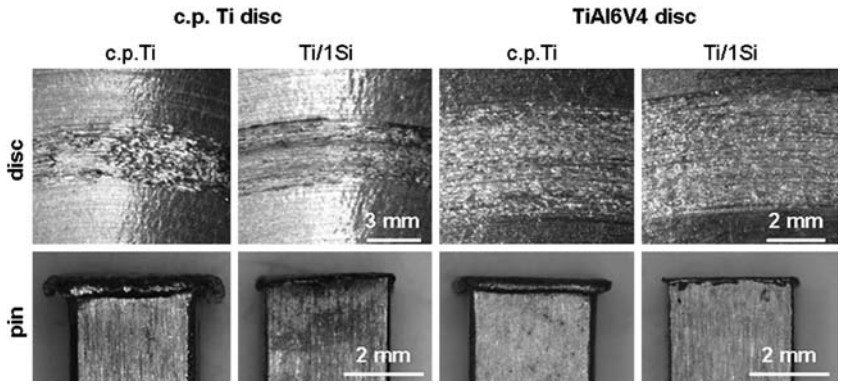

Fig. 8 Optical microscopy images of c.p. Ti and Ti/1Si pins and the discs after the wear tests

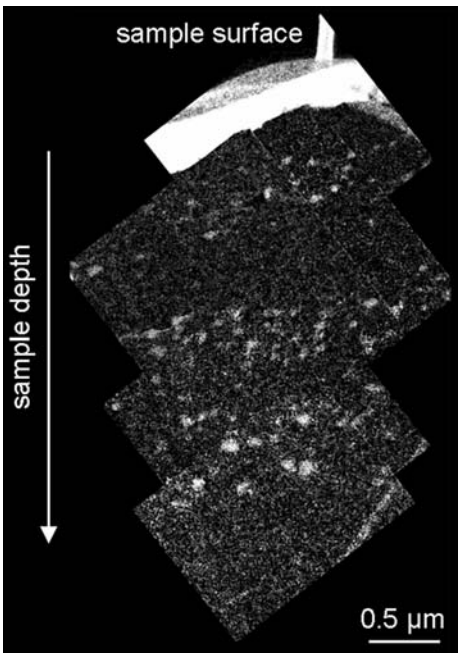

Fig. 9 EELS carbon distribution image (TiC_x) of the Ti/2.6HMDS pin surface after wear test as a function of the sample depth

SPD-c.p. Ti with the novel dispersion strengthened materials. The grain size refinement causes a decrease in the wear coefficient from 5.5×10^{-5} mm^3 N^{-1} m^{-1} to 3.2×10^{-5} mm^3 N^{-1} m^{-1}. An additional decrease to approx. 1×10^{-5} mm^3 N^{-1} m^{-1} was obtained with the dispersoids, but there was no influence of volume fraction and size.

Biological compatibility of the wear particles

The release of the pro-inflammatory cytokines IL-8 and the expression of cell adhesion molecules ICAM-1 after 24 h exposure are shown in Fig. 12 to describe the inflammatory foreign body reactions originated in the endothelial cells. Heavy inflammation (positive control) is caused by divalent cobalt ions. The release of IL-8 and the expression of

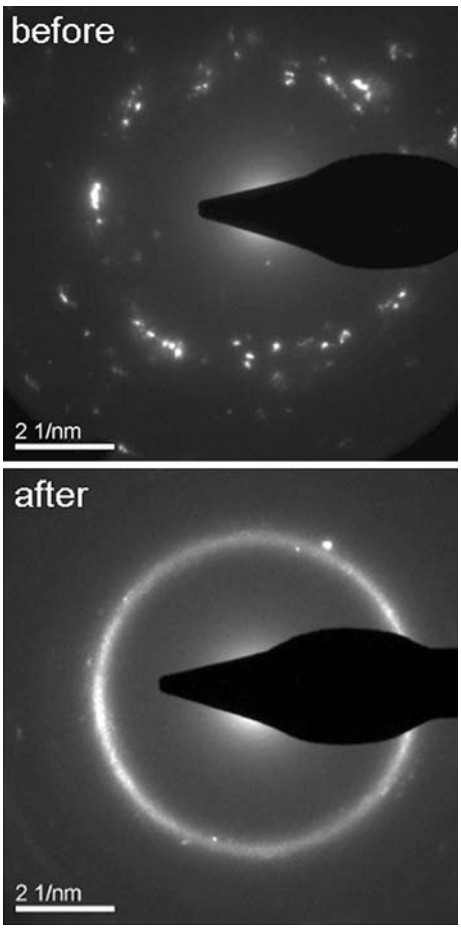

Fig. 10 TEM electron diffraction patterns of Ti/2.6HMDS before and after wear testing

ICAM-1 are slight and increase with the concentration of the particles and their internalization. The effects are only slightly higher for the wear particles with TiC_x than for the other particles tested. However, in comparison to the positive control, the effects are small and of no relevance. The metabolic cell activity characterized by MTS conversion and number of cells is not significantly affected by the exposure to the different wear particles (Fig. 13). The negative influence of TiAl6V4 on cells [14, 15], that in

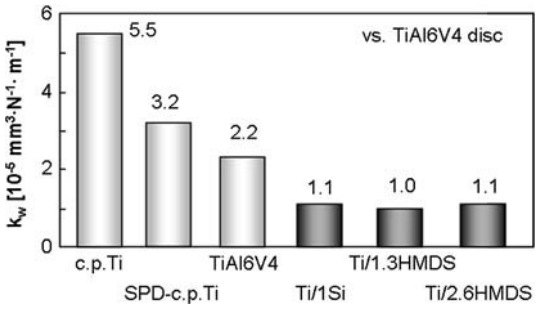

Fig. 11 Wear coefficient of titanium materials tested versus TiAl6V4 disc

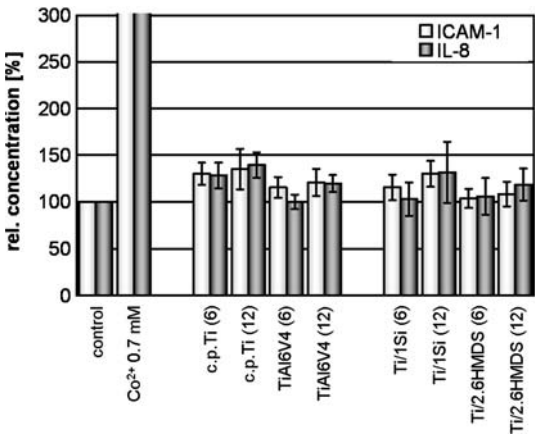

Fig. 12 IL-8 release and ICAM-1 expression after 24 h exposure for different particle concentrations; 6 and 12 µg particles per ml medium, respectively

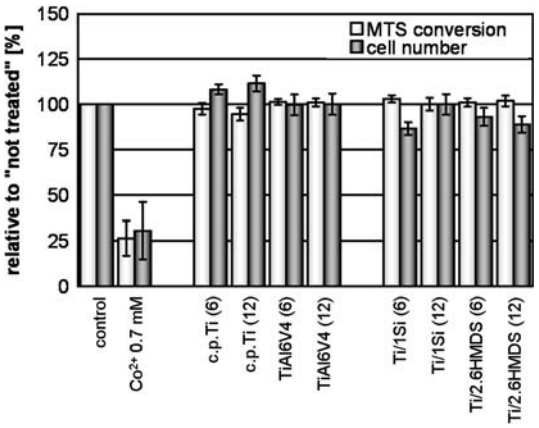

Fig. 13 MTS conversion and cell number after 72 h exposure for different particle concentrations; 6 and 12 µg particles per ml medium, respectively

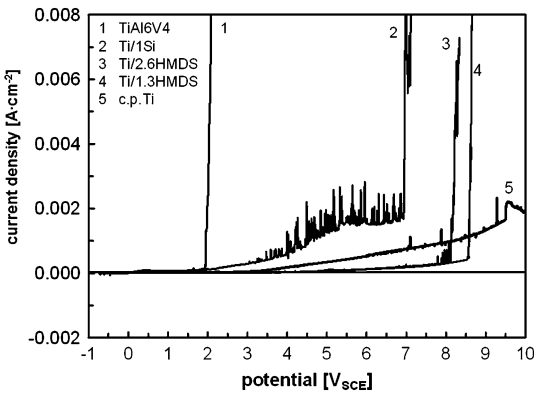

Fig. 14 Current density-potential-plots of titanium materials as result of potentio-dynamic measurements (10 mV s^{-1})

literature is attributed to the toxic effects of released vanadium ions [14] is not clearly proven by these tests. Therefore, we recommend that the biocompatibility of these new materials be assessed by other tests, e.g., as cited in [14].

Electrochemical behaviour

The excellent biocompatibility of titanium materials comes from the spontaneously forming protective passive layers. These layers, approximately 3 nm in thickness on polished or grinded surfaces, consist of a substochiometric titanium oxide of the general formula $Ti_{1+x}O_2$ [16]. Titanium oxide is characterized by *n*-type semiconductor properties that are important for the use as implant material because charge transfer processes (electrons, ions) between the implant and the human body tissue, which can result in conformational changes of biomolecules and immunological reactions, are inhibited [17, 18].

As shown in Fig. 14, all tested materials behave passively in the region of the normal redox potential of biological systems (350–550 mV_{SCE} [19]); corrosion current densities of 1.9–3.2 µA cm^{-2} were measured. For TiAl6V4, the trans-passive region, characterized by an increase of the current density, begins at 1.9 V_{SCE}. This is apparently due to the dissolution of the β-phase [20]. For the new ultrafine-grained and dispersion strengthened titanium materials active/passive transitions were observed at much higher potentials after continued polarization (Table 3). As expected from literature [21], c.p. Ti shows no break through of its passive layer until the maximum potential (10 V_{SCE}) of the experiment was reached. The lower break through potentials of the novel materials are probably the result of the ultrafine microstructure and the dispersoids that are embedded in the titanium oxide layer. However, the break through potentials of the ultrafine-grained and dispersion strengthened titanium materials are

Table 3 Results of the potentio-dynamic and EIS measurements

	c.p.Ti	TiAl6V4	Ti/1Si	Ti/1.3HMDS	Ti/2.6HMDS
Break trough potential [V_{SCE}]	>10	2	6.9	8.6	8.2
Flatband potential [mV_{SCE}]	110	226	63	93	115
Donor density [10^{20} cm^{-3}]	3.09	4.49	2.03	1.72	1.75

much higher than those of TiAl6V4 and clearly higher than the normal redox potential of biological systems (Table 3).

The *n*-type semiconductor properties of the titanium oxide passive layer can be described by the flatband potential U_{FB} and the donor density N_D determined in EIS by the Mott-Schottky-equation 2, where C is the capacity, C_{SC} is the space charge capacity in the *n*-type semiconductor, q is the charge of electron, ε is the relative dielectric constant, ε_0 is the absolute dielectric constant, U is the impressed potential and k is the Boltzmann constant [9, 16].

$$\frac{1}{C_{SC}^2} = \frac{2}{q \cdot \varepsilon \cdot \varepsilon_0 \cdot N_D} \cdot \left(U \cdot U_{FB} - \frac{k \cdot T}{q} \right) \approx \frac{1}{C^2} \qquad (2)$$

In *n*-type semiconductors, the concentration of electrons is decreased for $U_{FB} < U_{Redox}$ and the difference between the flatband potential and the redox potential of biological systems is a measure of the inhibition of charge transfer by electrons [16]. In this case, the charge transfer I_{Redox} is only a function of the defects in the oxide layer (described by the donor density N_D), that can be influenced e.g., by the microstructure, alloying elements or sample preparation.

The capacities depending on the existing potentials resulting from the EQUIVCRT evaluations are shown in Fig. 15. Also displayed is the applied equivalent circuit diagram. The flatband potentials U_{FB} and donor densities N_D, determined from these graphs, are presented in Table 3. It can be seen that the U_{FB} of the newly developed titanium materials is not raised in comparison to that of c.p. Ti. It therefore seems that the refined microstructure and the dispersoids are obviously not affecting the *n*-type semiconductor properties of the titanium oxide passive layer. TiAl6V4 shows a raised flatband potential in comparison to the other tested materials. However, it is also lower than the normal redox potential of biological systems. All determined donor densities are within the same order of magnitude, i.e., the differences between them are only slight. Regarding investigations on TiAl6Nb7 [16], the present work shows similar results for the newly developed titanium materials (Ti/1Si, Ti/1.3HMDS, Ti/2.6HMDS) in comparison to TiAl6V4. This makes them more suitable than TiAl6V4 for the use as implant material in the human body. Yet further electrochemical tests must be performed to characterize the depassivation/passivation behaviour of the new titanium materials. It is well-known that Ti can be depassivated by a short period in reducing conditions. The subsequent passivation rate is influenced by alloying elements [22]. This might have a significant impact on the stability of the materials in living tissue.

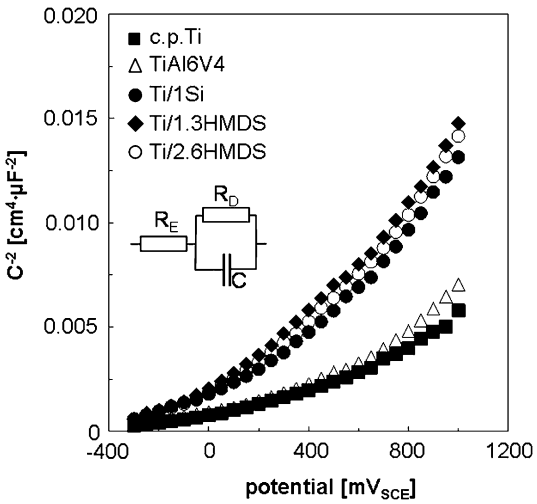

Fig. 15 Mott–Schottky plots for the passive layers of the titanium materials measured by EIS in PBS at 37 °C (R_E, Ohmic resistance of the electrolyte; R_D,charge transfer resistance; C, capacity)

Conclusions

Our investigations have shown that ultrafine-grained and dispersion-strengthened titanium materials can be developed by powder metallurgical methods. Either silicon powder or the organic fluid hexamethyldisilane were milled with titanium powder. All developed materials consisted of an ultrafine-grained titanium matrix with extremely fine dispersoids, and exhibited high hardness and strength. The material Ti/1.3HMDS (wt.%) is characterized by excellent ductility as result of a bimodal grain size distribution. As shown in the wear tests, the wear resistance in comparison to c.p. Ti and implant alloy TiAl6V4 could be significantly increased along with the high hardness and strength of the new materials. The wear particles of the novel titanium materials, generated during the tribological tests, showed no negative effects to the biocompatibility compared to c.p. Ti. They neither caused increased inflammatory reactions of human dermal endothelial cell nor did they affect their vitality.

The electrochemical behaviour of the new materials is only insignificantly deteriorated to that of c.p. Ti. Their break through potentials are lower than that of c.p. Ti, but far above the normal redox potential of biological systems. The semiconductivity of the titanium oxide passive layer is not influenced, both flatband potential and donor density are comparable to that of c.p. Ti.

In summary, it can be stated that Ti/1.3HMDS shows the most interesting combination of properties for application as implant material.

Acknowledgements The authors would like to thank Y. Grin, N. Reinfried (MPI Dresden), G. Walther (IFAM Dresden), T. Gemming (IFW Dresden) and K. Peters (Mainz University) for the technical support and fruitful discussions. The financial support by the Deutsche Forschungsgemeinschaft (Schwerpunktprogramm 1100) is gratefully acknowledged.

References

1. Breme HJ (1996) In: Peters M, Leyens C, Kumpfert J (eds) Titan und Titanlegierungen. DGM Informationsgesellschaft mbH
2. Wintermantel E, Ha S-W (1998) Biokompatible Werkstoffe und Bauweisen, 2., vollst. neubearb. Aufl. Springer, Heidelberg
3. Sauer C, Weißgärber T, Dehm G, Mayer J, Püsche W, Kieback B (1998) Z Metallkd 89:119
4. Tokita M (1999) Mater Sci Forum 308–311:83
5. Handtrack D, Sauer C, Kieback B (2004) Proc PM2004 World Congr, Vienna 419
6. Handtrack D, Despang F, Sauer C, Kieback B, Reinfried N, Grin Y (2006) Mat Sci Eng A 437:423
7. Handtrack D (2006) Dissertation, Technische Universitaet Dresden (submitted in Sept. 2006)
8. Boukamp BA (1993) Equivalent Circuit, Version 4.51, University of Twente
9. Pan J, Leygraf C, Thierry D, Ektessabi AM (1997) J Biomed Mater Res 35:309
10. Schubert-Bischoff P, Bloeck U, personal communication
11. Koch CC, Youssef KM, Scattergood RO, Murty KL (2005) Adv Eng Mater 7(9):787
12. Han BQ, Lavernia EJ (2005) Adv Eng Mater 7(6):457
13. Wang Y, Chen M, Zhou F, Ma E (2002) Nature 419:912
14. Eisenbarth E, Meyle J, Nachtigall W, Breme J (1996) Biomat 17:1399
15. Spyrou P, Papaioannou S, Hampson G, Brady K, Palmer RM, McDonald F (2002) Clin Oral Impl Res 13:623
16. Scharnweber D, Beutner R, Roeßler S, Worch H (2002) J Mater Sci: Mater Med 13:1215
17. Thull R (1998) In: Helsen JA, Breme HJ (eds) Metals as Biomaterials. John Wiley, New York, p 289
18. Scharnweber D (1998) In: Helsen JA, Breme HJ (eds) Metals as Biomaterials. John Wiley, New York, p 101
19. Velten D, Biehl V, Aubertin F, Valeske B, Possart W, Breme J (2002) J Biomed Mater Res 59:18
20. Schmidt H, Exner HE (1999) Z Metallkd 90:594
21. Zwicker U (1974) Titan und Titanlegierungen. Springer Verlag, Berlin
22. Khan MA, Williams RL, Williams DF (1996) Biomat 17:2117